Impact Factor : 4.7
Q2

Journal of Molecular Structure 1353 (2026) 144785

Contents lists available at ScienceDirect

Journal of Molecular Structure

journal homepage: www.elsevier.com/locate/molstr

Design, synthesis, and evaluation of fused Indolin-2-one derivatives as potent anti-inflammatory and anti-cancer agents targeting the CXCR6 pathway

Wanhui Dai [a], Dongwei Zhu [b], Kanagaraj Rajalakshmi [b], Natarajan Kiruthiga [c], Sudhakar Pachiappan [d], Panneerselvam Theivendren [e,*], Selvaraj Muthusamy [b,*], Siyi Wu [f,*], Yang Jiang [g,*]

[a] Department of Clinic Laboratory, The Second Hospital of Nanjing, Nanjing University of Chinese Medicine, Nanjing 210000, Jiangsu, PR China
[b] Department of Immunology, Jiangsu Key Laboratory of Laboratory Medicine, School of Medicine, School of Chemistry and Chemical Engineering, Jiangsu University, Zhenjiang, 212013, PR China
[c] Department of Pharmaceutical Chemistry, KMCH college of Pharmacy, Kalappatti road, Coimbatore, 641048, Tamil Nadu, India
[d] Department of Pharmacology, Swamy Vivekananda College of Pharmacy, Elayampalayam, Namakkal, Tamil Nadu 637205, India
[e] Department of Pharmaceutical Chemistry & Analysis, School of Pharmaceutical Sciences, Vels Institute of Science, Technology & Advanced Studies, Pallavaram, Chennai, Tamil Nadu 600117, India
[f] Clinical Laboratory Center, The Affiliated Taizhou People's Hospital of Nanjing Medical University, Taizhou 225300, Jiangsu, PR China
[g] Department of Clinical Laboratory, Xuzhou Central Hospital, 221009 Xuzhou, Jiangsu, China

ARTICLE INFO

Keywords:
Indolin-2-one derivatives
CXCR6 receptor
Molecular docking
Inflammation
Molecular dynamics
Anti-cancer activity

ABSTRACT

The pathological condition known as cancer requires inflammatory processes for tumor growth while simultaneously impairing immune system monitoring. The research presents an analysis of heterocyclic compound synthesis and assessment including fused pyrazole and indolin-2-one derivatives. The researchers performed additional in silico and *in vivo* analysis on compounds 5a and 5i from the designed heterocyclic compounds. Performed using graph theoretical methods the investigators identified CXCR6 as a potential key target for therapy. The binding affinity evaluation of 5a and 5i showed strong interactions with CXCR6 receptors which exceeded the binding capacity of Celecoxib. The interactions between the receptor and ligands 5a and 5i exhibited notable stability over a 100 ns simulation period, as revealed by molecular dynamics analysis. Further extended simulations of the 6KVA–5a complex over 1000 ns provided valuable insights into the system's stability, highlighting key structural features. The analysis of RMSD, RMSF, and protein-ligand contact profiles demonstrated consistent structural stability, residue flexibility, and identified crucial binding interactions, reinforcing the reliability of the receptor-ligand binding. The drug-likeness aspects and electronic stability of synthesized compounds received backing from density functional theory and SwissADME predictions. Results from carrageenan-induced paw oedema tests showed 5a and 5i reduced inflammation in living conditions in the same way as Diclofenac but 5a produced 48.57 % inhibition while Diclofenac reached 52.85 % inhibition. The study indicates that compound 5a demonstrates particular efficacy as a potential lead drug candidate for future anti-inflammatory treatment development through CXCR6 inhibition.

1. Introduction

A harmful stimulus activates the complex inflammatory response which starts from pathogens or damaged cells or irritants. The immune system and tissue repair function depend on inflammation but its persistent form leads to multiple disease developments including cancer [1–4]. Inflammatory processes within cancer cells develop tumor-promoting tissue conditions that drive cellular growth and the formation of blood vessels and cancer spread whereas they simultaneously block immune system monitoring. The inflammatory effects of

* Corresponding authors.
E-mail addresses: tpsphc@gmail.com (P. Theivendren), rajselva311@ujs.edu.cn (S. Muthusamy), 2930339808@qq.com (S. Wu), jy1241228831@qq.com (Y. Jiang).

https://doi.org/10.1016/j.molstruc.2025.144785
Received 8 September 2025; Received in revised form 7 November 2025; Accepted 17 November 2025
Available online 19 November 2025

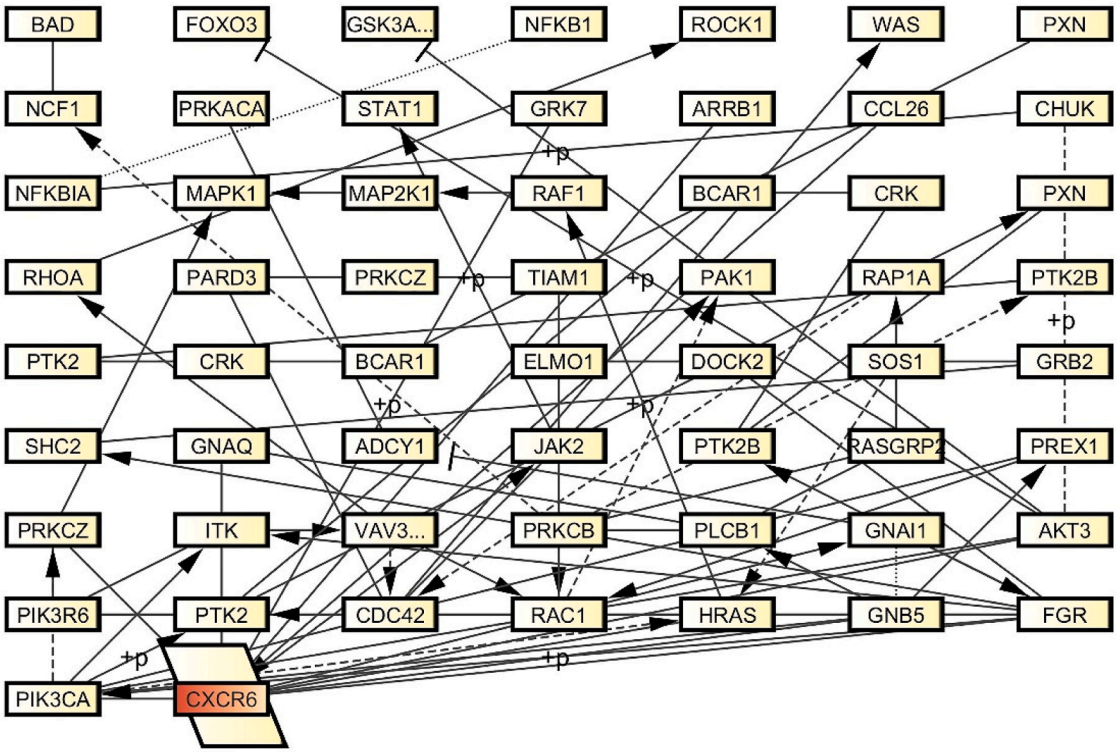

Fig. 1. Interaction network of CXCR6 and associated signalling molecules involved in chemokine signalling, showing protein–protein interactions, phosphorylation events, and regulatory nodes contributing to immune response and cellular signalling cascades.

Table 1
The results of network analysis with threshold parameter values.

Label	Degree	Betweenness	Closeness	Eccentricity	EigenVector	Radiality	Stress
CXCR6/Chemokine	12	944.0443	0.007299	0.125	0.439326	9	2262
FGR	9	584.7075	0.006944	0.111111	0.373908	8.877193	1574
PIK3CA	9	722.8035	0.007874	0.142857	0.425905	9.175439	1824
PTK2	5	155.8221	0.005952	0.125	0.216215	8.684211	448
GNB5	5	525.3959	0.006803	0.166667	0.243112	8.824561	1544
CDC42	5	325.54	0.005025	0.125	0.01427	7.912281	598
AKT3	5	494	0.00625	0.111111	0.18449	8.596491	1004
HRAS	5	286.0268	0.006135	0.111111	0.226833	8.54386	874
RAC1	5	294.9494	0.005682	0.111111	0.043618	8.315789	564
PIK3R6	5	90.51833	0.005814	0.1	0.235612	8.385965	316
PLCB1	4	575.5103	0.005882	0.166667	0.071534	8.421053	1830
GNAI1	4	231.2901	0.006494	0.125	0.208358	8.701754	372
VAV3	4	468.9595	0.005682	0.111111	0.052148	8.315789	876
ITK	4	426.4313	0.006289	0.111111	0.206495	8.614035	852
PRKCB	4	474.3308	0.004878	0.142857	0.018399	7.807018	1402
PRKCZ	4	159.6648	0.00641	0.2	0.217477	8.894737	540
RASGRP2	3	152.3333	0.00495	0.142857	0.018248	7.859649	282
PTK2B	3	79.44365	0.005181	0.1	0.08669	8.245614	274
PREX1	3	267.0604	0.006897	0.2	0.135306	8.859649	458

chemotherapy and radiation therapy frequently lead to worse side effects which harms patient recovery processes[5–7]. The management of inflammation remains essential in cancer treatment because it both strengthens therapeutic methods and minimizes treatment-related problems for improved patient success. The small proteins known as chemokines which function as “chemotactic cytokines” measure between 8 and 14 kDa in size. The proteins maintain similar regions that include four cysteine elements which form disulfide bonds through linkage. Chemokines receive their group classifications as CC, CXC, C or CX3C based on various cysteine patterns positioned at their N-terminal section [8–13]. Inflammation triggers inflammatory chemokines to create G-protein-coupled receptor signals that lead immune cells including monocytes and lymphocytes and neutrophils to move through chemotaxis. The chemokine receptors CCR1, CCR2, CCR3, CCR5, CXCR1, CXCR2, CXCR3, ACKR1, ACKR2 along with other receptors respond to these chemokines for interactions. Disrupted chemokine levels serve as an indicator in the development of multiple inflammatory diseases. CXCR6 neuralization effectively protects patients in conditions including lung ischemia-reperfusion injury and glomerulonephritis as well as pleuritis since these conditions are driven by neutrophil inflammatory response which resembles bacterial pneumonia[14]. The vital position of chemokines in inflammation activity has made them a great potential therapeutic choice. Conducting research to restrain chemokines might present a valuable approach in managing inflammatory processes. NSAIDs prevent chemokine production yet they trigger gastrointestinal harm since they minimize useful prostaglandin

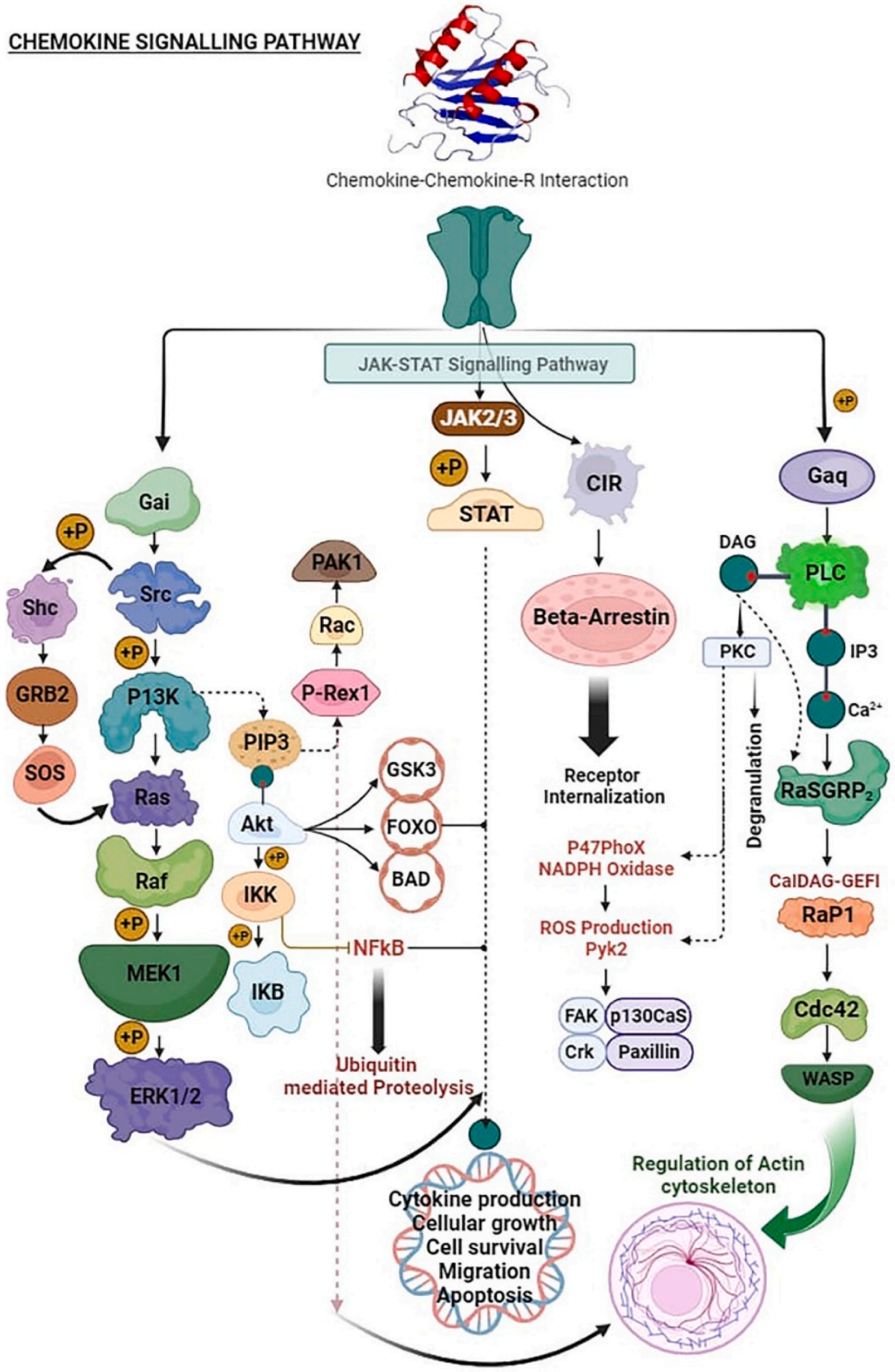

Fig. 2. Overview of the chemokine signalling pathway highlighting key molecular cascades involved in cytokine production, cell survival, ROS generation, receptor internalization, and cytoskeletal regulation through multiple signalling axes.

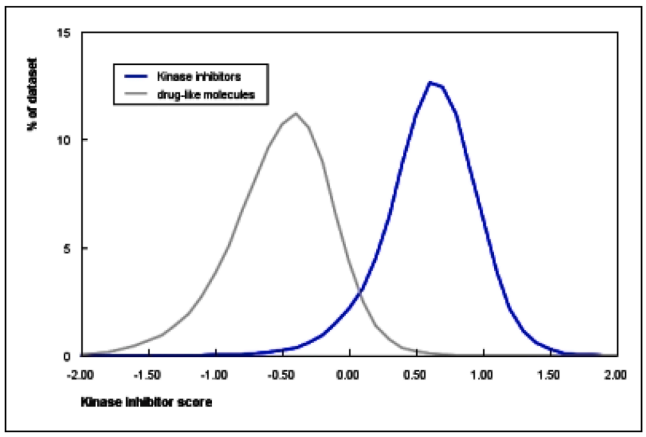

Fig. 3. Druglikeness comparison of compounds 5a–5l showing kinase inhibitor scores. The distribution illustrates a higher scoring trend (blue) for kinase inhibitors compared to general drug-like molecules (grey).

Table 2
The docking score and amino acid interaction of **5a-5l**.

Code	R	Score
5a	**4-Cl**	**−10.8**
5b	4-CF_3	−10.3
5c	4-NO_2	−10.3
5d	4-CH_3	−10.7
5e	4-NH_2	−9.7
5f	4-OH	−10.2
5 *g*	4-Cl	−10.6
5h	4-CF_3	−10.7
5i	**4-NO_2**	**−11.5**
5j	4-CH_3	−10.0
5k	4-NH_2	−10.8
5l	4-OH	−10.2
Acetaminophen		−5.1
Celecoxib		−8.7
Diclofenac		−6.7
Indomethacin		−7.3
Naproxen		−6.8
Ibuprofen		−6.9
Aspirin		−5.4

functions[15–17]. Drug designers have started using heterocycle-fused scaffolds because they show potential for multiple biological activities including anti-inflammatory and anti-cancer properties as well as anti-psychotic as well as anti-diabetic effects. Research on indoline as a scaffold has clearly demonstrated its established anti-inflammatory functions [18–21]

The study investigates the potential of innovative indolin-2-one derivatives, in particular compounds 5a and 5i, as anti-inflammatory agents with the target of the receptor (CRXC6). Through a series of in-silico and in-vivo evaluations, these compounds showed high binding affinities with the target, which was higher than the traditional anti-inflammatory drugs, Celecoxib. The compounds exhibited significant inhibition in the carrageenan induced paw edema model with compound 5a exhibiting a similar inhibition rate to Diclofenac. This research indicates that these derivatives, especially 5a, could be suitable lead candidates for the development of new anti-inflammatory drugs in the future, targeting the pathways involved in the activity of the receptor (CXCR6) and achieving better therapeutic results. The objective of this study is to design, synthesize, and evaluate fused indolin-2-one derivatives as potent anti-inflammatory and anti-cancer agents targeting the CXCR6 pathway. The compounds were subjected to in-silico and in-vivo analyses, revealing strong interactions with CXCR6 receptors. The study highlights compound 5a as a promising lead for future therapeutic development.

2. Materials and methods

2.1. Materials

The laboratory obtained all chemicals and reagents from established suppliers Qualigens and E. Merck India Ltd. alongside CDH and SD Fine Chem. Before use the research team purified solvents coming from laboratory reagent quality sources. A thin-layer chromatography investigation occurred through the utilization of silica gel G obtained from E. Merck India Ltd. Open capillary methods were used to determine melting points which exist as uncorrected values. Standard spectroscopic equipment performed the characterization process. The 500 MHz proton nuclear magnetic resonance spectra obtained through a Bruker Avance-500 spectrometer used $CDCl_3$ as solvent with tetramethylsilane (TMS) as a reference standard. The JEOL-SX-102 instrument evaluated samples by means of electron impact (EI) ionization procedures. Jasco FT-IR 410 spectrometer analyzed the spectra using KBr pellets. Perkin Elmer 2400C analyser performed elemental analysis which showed

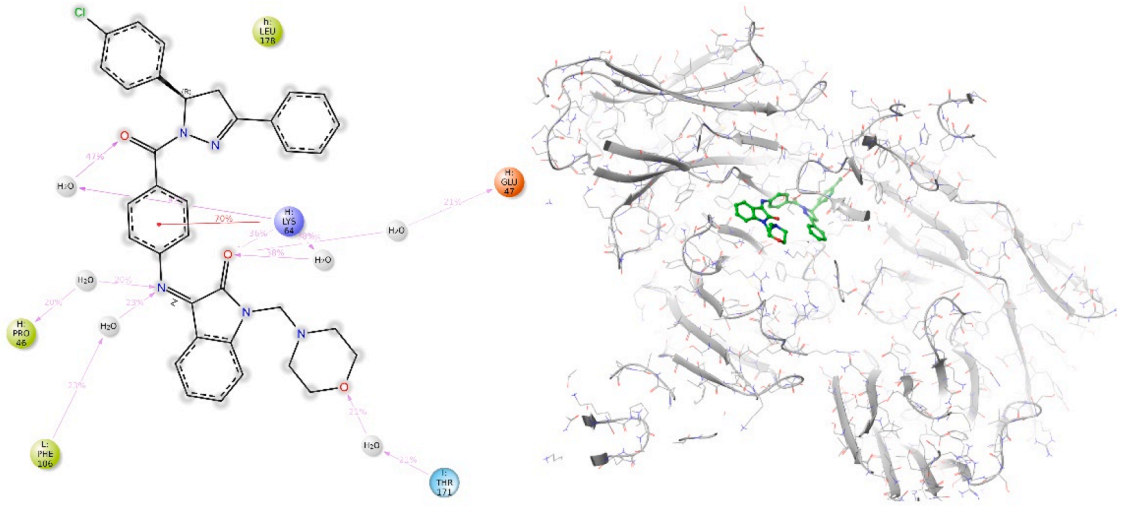

Fig. 4. 2D and 3D interaction diagrams of compound 5a with the target protein, showing key hydrogen bonds, hydrophobic interactions, and binding conformation within the protein's active site.

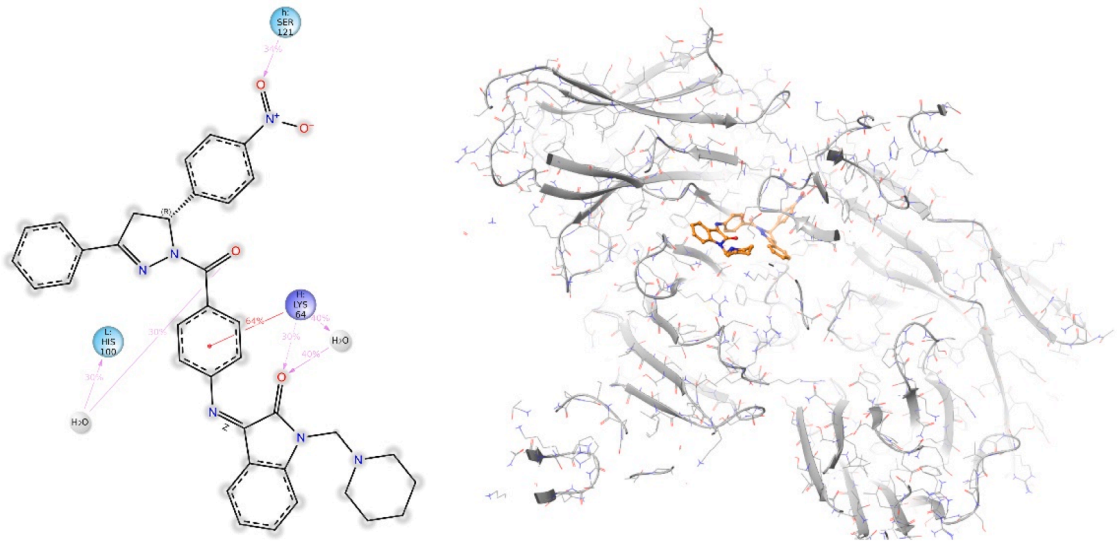

Fig. 5. 2D and 3D binding interaction diagrams of test compound 5i showing hydrogen bonding, π–π stacking, and hydrophobic contacts within the active site pocket of the target protein.

experimental results close to theoretical values with maximum deviations at ±0.4 %.

2.2. Methods

2.2.1. Graph theoreticalanalysis

A graph theoretical assessment of human inflammatory mediator proteins (KEGG pathway hsa:04,062) identified vital inflammatory mediators. The research team obtained KEGG pathway hsa:04,062 data from the KEGG database [22] through https://www.genome.jp/pathway/ hsa04062.

2.2.2. Drug-likeness analysis

The evaluation of drug-likeness properties for compounds 5a through 5l used Molinspiration software (https://www.molinspiration.com) that refers to standard drug structures for its evaluation [14,23]

2.2.3. Protein preparation

Data regarding the CXCR6 chemokine receptor (6KVA PDB ID) originates from RCSB Protein Data Bank at https://www.rcsb.org/. Protein preprocessing involved water molecule removal and missing residue addition through CHARMM-GUI [14,23]. website (https://www.charmm-gui.org/).

2.2.4. Ligand preparation

Compounds 5a–5l along with reference NSAIDs Acetaminophen, Celecoxib, Diclofenac, Indomethacin, Naproxen, Ibuprofen were obtained from PubChem website (https://pubchem.ncbi.nlm.nih.gov/) in . sdf format [14,23]. The preparation process of ligands happened through BIOVIA Discovery Studio Visualizer (https://discover.3ds.com/discovery-studio-visualizer-download).

2.2.5. Molecular docking

The researchers performed molecular docking with AutoDock Vina through the PyRx interface. The pdbqt format conversion process took place before Auto Grid defined the docking grids. After calculating binding affinities Discovery Studio Visualizer was used to select the most favorable binding pose with the lowest free energy value.

2.2.6. Binding siteidentification

The PrankWeb server (https://prankweb.cz/) predicted active binding sites of CXCR6. The docking parameters for receptor grid generation in PyRx originated from these sites [14,23].

2.2.7. Molecular dynamicssimulation

MD simulations were performed using the Desmond module within the Schrödinger suite. The system was simulated in an orthorhombic box with periodic boundary conditions, and water molecules (TIP3P model) were added to fill the box. The Nose-Hoover thermostat and the Parrinello-Rahman barostat were used to maintain a constant temperature (300 K) and pressure (1 atm), respectively. A time step of 2 fs was employed, with electrostatic interactions treated using the Particle Mesh Ewald (PME) method and a cutoff of 9 Å for van der Waals interactions. Bond lengths involving hydrogen atoms were constrained using the LINCS algorithm. Protonation states of titratable residues were determined at a pH of 7.4 using the PROPKA method [24,25].

2.2.8. Density functionaltheory (DFT) analysis

The energy minimization technique was carried out for selected compounds (5a, 5i) together with standard Celecoxib by using Spartan'14. The GaussView 6.0.16 software computed HOMO-LUMO energy values but the researcher converted Hartree units to obtain electronic stability information through energy gap measurements expressed in eV [14,23].

2.2.9. ADME and pharmacokineticmodelling

The SwissADME tool (http://www.swissadme.ch/) predicted in silico ADME properties that included molecular weight together with solubility and bioavailability and GI absorption and BBB penetration and ten physicochemical descriptors [14,23,26,27].

2.2.10. Synthesis of targetcompounds

The sequence of chemical reactions needed several individual steps. The combination of isatin, formaldehyde and morpholine/piperidine in ethanolic solution went through selective reflux before obtaining solid crystals from the product. Equimolar refluxing of 2 together with p-amino benzoic acid occurred in ethanol. The researchers transformed 3 into acid chlorides through thionyl chloride treatment and reactors them with ethanol hydrazine to yield the resulting hydrazides 4. The condensation of various aldehydes with acetophenone took place in an ethanol solution where NaOH served as the base. The reaction between chalcones and hydrazides 4a/4b in refluxing DMF led to the formation of final products **5a** and **5i** while recrystallization served as purification method.

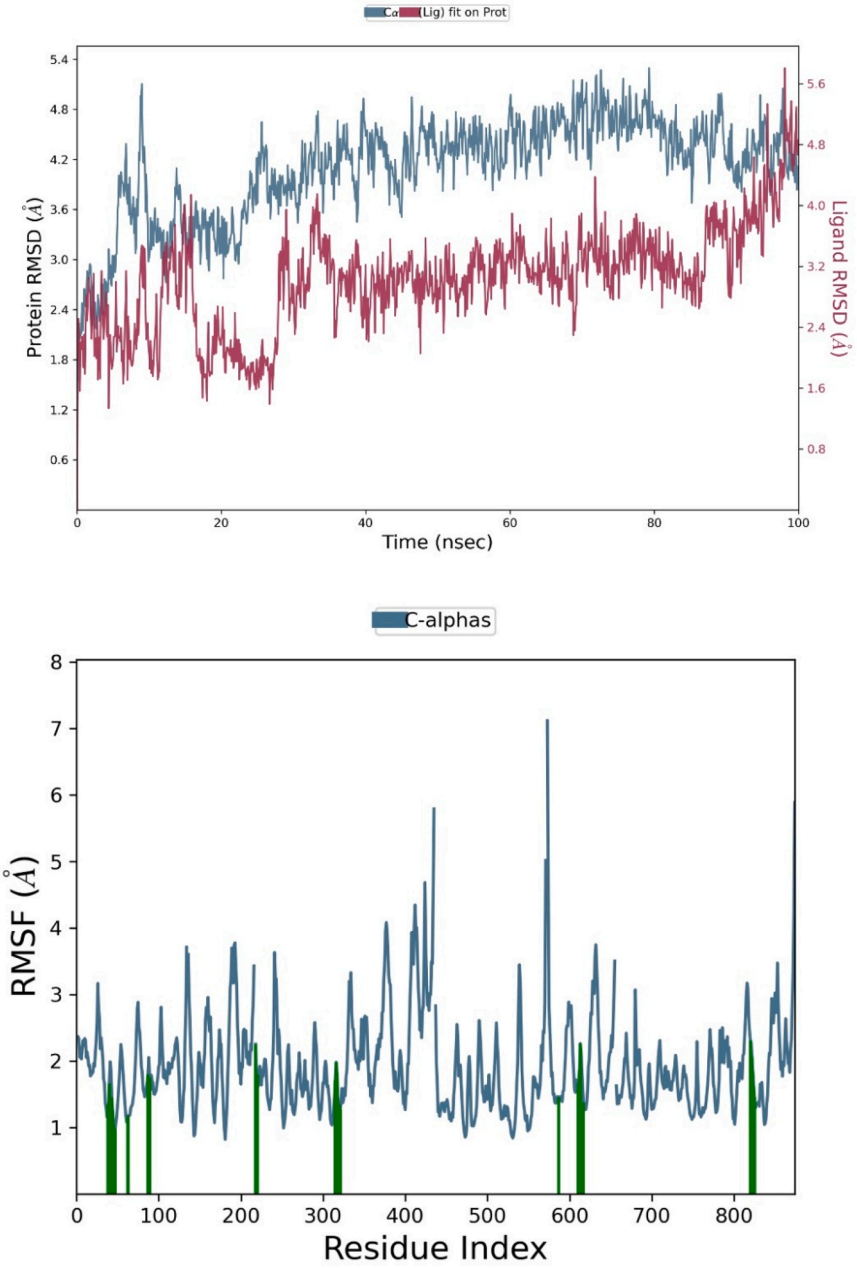

Fig. 6. Molecular dynamics simulation analysis showing RMSD of protein-ligand complex over 100 ns (top) and RMSF plot indicating residue-wise flexibility (bottom) of the protein C-alpha atoms of 6KVA-5a complex.

2.2.11. *Anti-inflammatory evaluation*

In vivo studies were conducted using male Sprague-Dawley rats (180–220 g), with 6–8 animals per group. Treatment groups included 5a (50 mg/kg), 5i (50 mg/kg), Diclofenac (15 mg/kg), and Celecoxib (6 mg/kg), all administered orally (p.o.). The control group received 0.5 % CMC (vehicle). Animals were randomly assigned to the treatment groups using a random number generator, and all assessments were conducted by investigators blinded to the treatment allocation. Exclusion criteria included any animal exhibiting signs of illness (*e.g.*, extreme weight loss, abnormal behavior, or inability to move) prior to or during the study period [28]. The study received Institutional Animal Ethics Committee (IAEC) under approval number SVCP/IAEC/PA/02/02/2022 prior to the experiment.

2.2.12. *MTT assay*

MTT assays were performed using a cell line seeded at a density of 1 × 10^4 cells/well in 96-well plates. After 24 h of incubation, cells were treated with five concentrations of the test compounds in triplicate. The compounds were dissolved in DMSO, and the final DMSO concentration did not exceed 0.1 %. After treatment, 100 μL of MTT solution (0.5 mg/mL) was added to each well, and the plates were incubated at 37 °C for 4 h. The formazan crystals formed were solubilized by adding 100 μL of DMSO. Absorbance was measured at 570 nm using a microplate reader. The IC_{50} values were calculated based on triplicate runs for each concentration [22,29,30].

2.2.13. *Statistical analysis*

A standard deviation combined with Mean served to display the results. The research utilized one-way analysis of variance (ANOVA) for performing overall statistical comparisons. The anti-inflammatory investigation employed Dunnett's multiple comparison tests as a follow-up analysis after one-way analysis of variance. The investigation

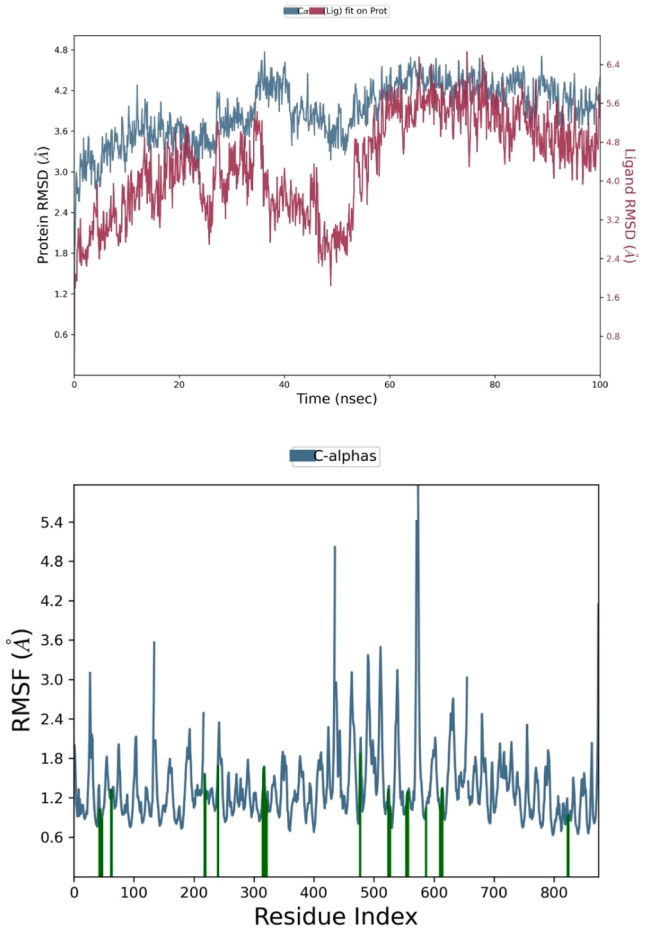

Fig. 7. RMSD (top) and RMSF (bottom) plots of the 6KVA–5i complex showing protein-ligand stability over 100 ns and residue-wise flexibility of the C-alpha atoms, respectively.

determined mean values as statistically significant whenever p-values fell under 0.05 ($p < 0.05$).

3. Results and discussion

3.1. Graph theoreticalanalysis

A graph model constructed through Homo sapiens proteomic inflammatory interaction study (hsa:04,062) contained 82 edges and 59 nodes as shown in Fig. 1 and listed in Table 1. The analysis conventionally relied on graphs for identifying key proteins through different centrality measurements. The network parameter analysis demonstrated that CXCR6/Chemokine functioned as the central motif because it exceeded other proteins across multiple centrality metrics which included Stress (2262) and Radiality (9) as well as Eigenvector centrality (0.439326) and Eccentricity (0.125) and Closeness (0.007299) and Betweenness (944.0443) and Degree (12). The strength of interactions between CXCR6 and FGR, PIK3CA, PTK2, GNB5, CDC42, AKT3, HRAS, RAC1 and other proteins made this target suitable for anti-inflammatory drug development. Additional investigations of CXCR6/Chemokine as the primary target will progress through virtual and biological testing based on these results.

3.2. Chemokine signallingpathway

The chemokine signalling pathway displays intricate sequences of molecular events starting from chemokine-receptor binding to generate various cellular effects. Chemokine engagement leads to G-protein activation of heterotrimeric Gαi and Gαq which gives rise to different signaling pathways that control transcription along with cytoskeletal changes and ROS formation and cellular survival. Generators Ras–Raf–MEK–ERK cascade as well as the PI3K–Akt–NFκB axis operate within the left arm to play essential roles in gene transcription and cytokine production and cell proliferation processes. When Ras becomes active through the bindings of GRB2–SOS it triggers MEK1 kinase activity that phosphorylates ERK1/2 proteins for activating genes that sustain cell growth and survival. When PI3K becomes activated, it phosphorylates Akt which causes FOXO and BAD inhibition and allows NFκB to activate the transcription of inflammatory and survival genes through IKK activation. When IKB undergoes ubiquitin-mediated degradation it enables NFKB to move into the nucleus which strengthens pro-survival together with pro-inflammatory responses. Gαq-PLC signaling creates DAG and IP3 which releases calcium to activate PKC and downstream molecules RaSGRP2 and RaP1. Actin cytoskeleton dynamics require Cdc42 and WASP in addition to the influence brought by these factors for immune cell movements and degranulation. The internalization process initiated by β-arrestin enables chemokine receptor signal modulation and grants ROS-producing capacity to Pyk2 while creating focal adhesion protein-mediated cytoskeletal regulation. Multiple integrated signalling pathways demonstrate the diverse effects of chemokine signalling which results in inflammation and immune cell attraction and apoptosis control and cytoskeletal alterations Fig. 2.

3.3. Drug-likeness analysis

The Molinspiration analysis established that all synthesised compounds 5a–5l matched drug-likeness conditions which define acceptable pharmaceutical structural features. The kinase inhibition bioactivity scores obtained favourable levels which demonstrate these compounds meet desirable criteria for pharmacological applications Fig. 3.

3.4. Molecular docking

Molecular docking analyses evaluated the binding efficacy between the experimental compounds (5a–5l) and reference anti-inflammatory drugs (Acetaminophen, Celecoxib, Diclofenac, Indomethacin, Naproxen and Ibuprofen) toward the CXCR6 receptor (PDB ID: 6KVA). The binding affinities of molecules 5a and 5i to the receptor exceeded those of Celecoxib by reaching –10.8 and –11.5 kcal/mol respectively. Each strong interaction between residues LYS64 (70 % π-interaction and 36 % with carbonyl oxygen in 5a) LYS64 (64 %) and SER121 (34 % with NO_2 group) in 5i increased the binding affinity of the compounds to the CXCR6 receptor. The interaction models in two and three dimensions are presented through Table 2 and Figs. 4 and 5.

3.5. Molecular dynamicssimulation

The Molecular Dynamics (MD) plots shown for RMSD (Root Mean Square Deviation), RMSF (Root Mean Square Fluctuation) and H-bond counts are useful to obtain insights into the stability and flexibility of protein-ligand interactions over time. In the RMSD plot, the stability of the protein and ligand complex are evaluated over the course of the simulation. The x-axis is the time in nanoseconds (ns) of the simulation and the y-axis is the RMSD values (in Å) of the protein and the ligand. It is clear from the plot that the complex of protein and ligand reaches stability after a certain period of time with fluctuations representing structural adjustments in the system. The plot can be improved by labeling the axes with greater clarity and using consistent time units for a more accurate comparison. The RMSF plot on the other hand, measures the flexibility of the protein structure by monitoring the fluctuations of the atomic positions over time. In the figure, the protein's residue index is plotted against the RMSF (in Å), which shows large variations at some

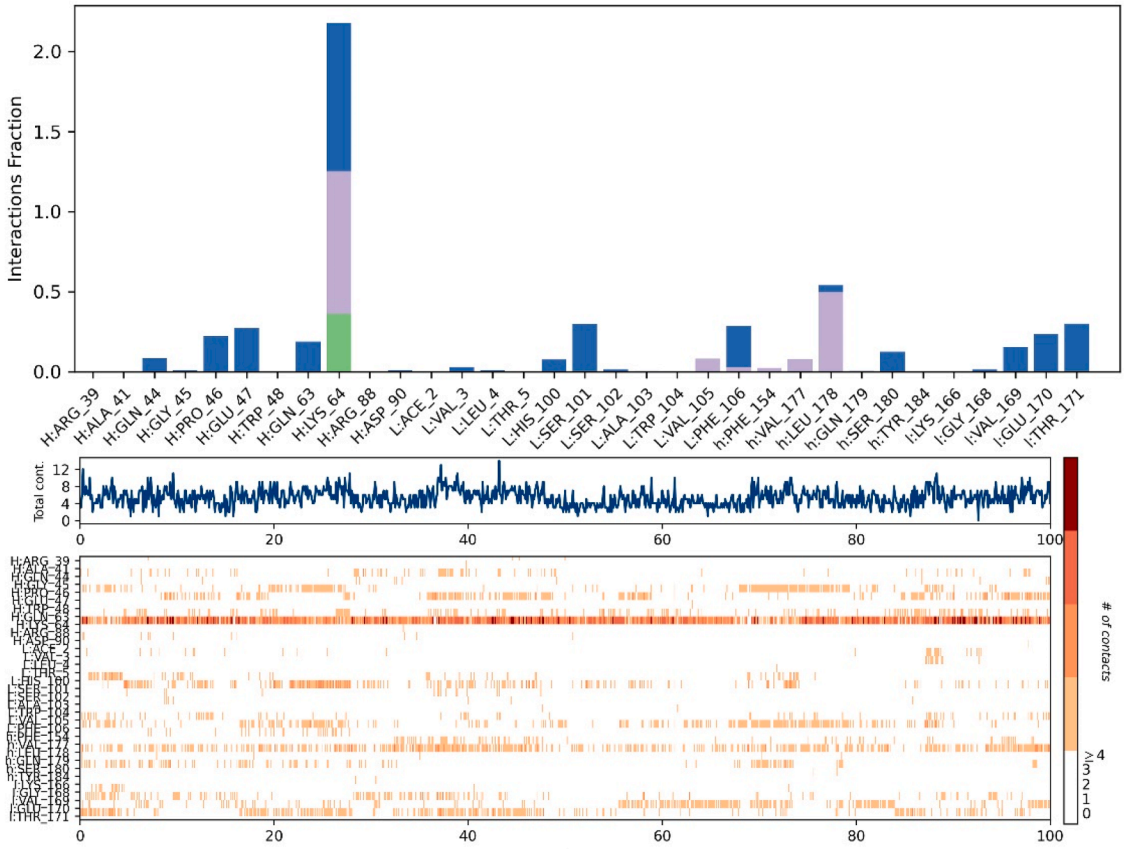

Fig. 8. Protein-ligand interaction analysis of the 6KVA–5a complex showing key residue H:LYS 64 involved in binding, contact frequency over 100 ns, and heatmap of intermolecular contacts throughout the simulation trajectory.

residues, which could be related to protein flexibility. The green markers indicate regions with greater fluctuations, which may indicate sites of interest for binding of a ligand or for a function. A visualization of number of hydrogen bonds between the protein and ligand during the simulation is provided on the H-bond count plot. Although informative, it would be great if the legend contained some information about the length of the trajectory and the smoothing method used with the data for greater clarity.

MD simulation activities evaluated the binding stability of 5a and 5i interacting with the CXCR6 protein. The simulation results exhibited both RMSD and RMSF values that remained unchanged throughout the 100 ns time period. Compound 5a showed protein ligand interaction ranges from 1.92 to 5.31 Å and 1.56–5.72 Å with the ligand during the assessment period. Both 5i interactions extended to 1.43 - 4.64 Å between the protein molecule while the ligand-maintained connections between 1.64–5.72 Å. Throughout the simulation period both amino acids LYS64 and SER121 maintained constant significant connections with each other (Figs. 6, 7, 8, 9).

The 5a compound displayed average trajectory values at Prot_CA equal to 4.089131 ns and 3.026948 ns at Lig_wrt_Protein but 5i showed values of 3.898315 ns and 4.352075 ns at Prot_CA and Lig_wrt_Protein, respectively. The data showed that 5a formed a stable complex structure than 5i. The torsional investigation showed sturdy rigid connections in 5a substance when linking the 3-phenyl, 4-chlorophenyl, and 1-carbonyl groups along with rigidity in the imino group yet flexibility in the 1-methyl group (Fig. 10). The rigidity-flexibility characteristics of 5i proved identical to the ones observed in 5a (Fig. 11).

The **1000 ns** simulation of 5a-CXCR6 produced enduring complex stability through both simulation runs and uninterrupted LYS64 interactions during the duration. The duration of the simulation showed no change in the powerful structural connections that bind the indolin-2-one and pyrazole core of molecule 5a (Figs. 12 and 13). Data from these tests prove that CXCR6 receptor complexes with 5a and 5i achieve stable associations that might make the compounds viable anti-inflammatory treatment leads.

3.6. MM-GBSA analysis

The energy decomposition analysis for both Indolin-2-one (5a) and Indolin-2-one (5i) provides insightful findings regarding their binding interactions. As shown in Fig. 6, Indolin-2-one (5a) has a total energy of −43.0 kcal/mol, with the van der Waals interaction contributing the most, amounting to −54.0 kcal/mol. The electrostatic energy for this compound is calculated at −20.0 kcal/mol, while the polar solvation and nonpolar solvation energies were −10.0 kcal/mol and −41.0 kcal/mol, respectively. This suggests a relatively stable binding of 5a with the target protein, primarily driven by favorable van der Waals forces, while the nonpolar solvation seems to contribute to destabilization.

For Indolin-2-one (5i), the total energy is −62.0 kcal/mol, with van der Waals interactions again being the most dominant at −66.0 kcal/mol. The electrostatic interaction for 5i is slightly less favorable at −23.0 kcal/mol. The polar solvation and nonpolar solvation energies for 5i are −12.0 kcal/mol and −39.0 kcal/mol, respectively. The higher overall binding energy in 5i, compared to 5a, is due to the stronger van der Waals attraction and a more favorable electrostatic contribution, which might indicate a more stable interaction with the target Figs. 14.

3.7. Density functionaltheory (DFT) analysis

The assessment of 5a and 5i electronic stability by DFT calculations involved HOMO-LUMO (Highest Occupied Molecular Orbital - Lowest Unoccupied Molecular Orbital) energy gap analysis. The calculated

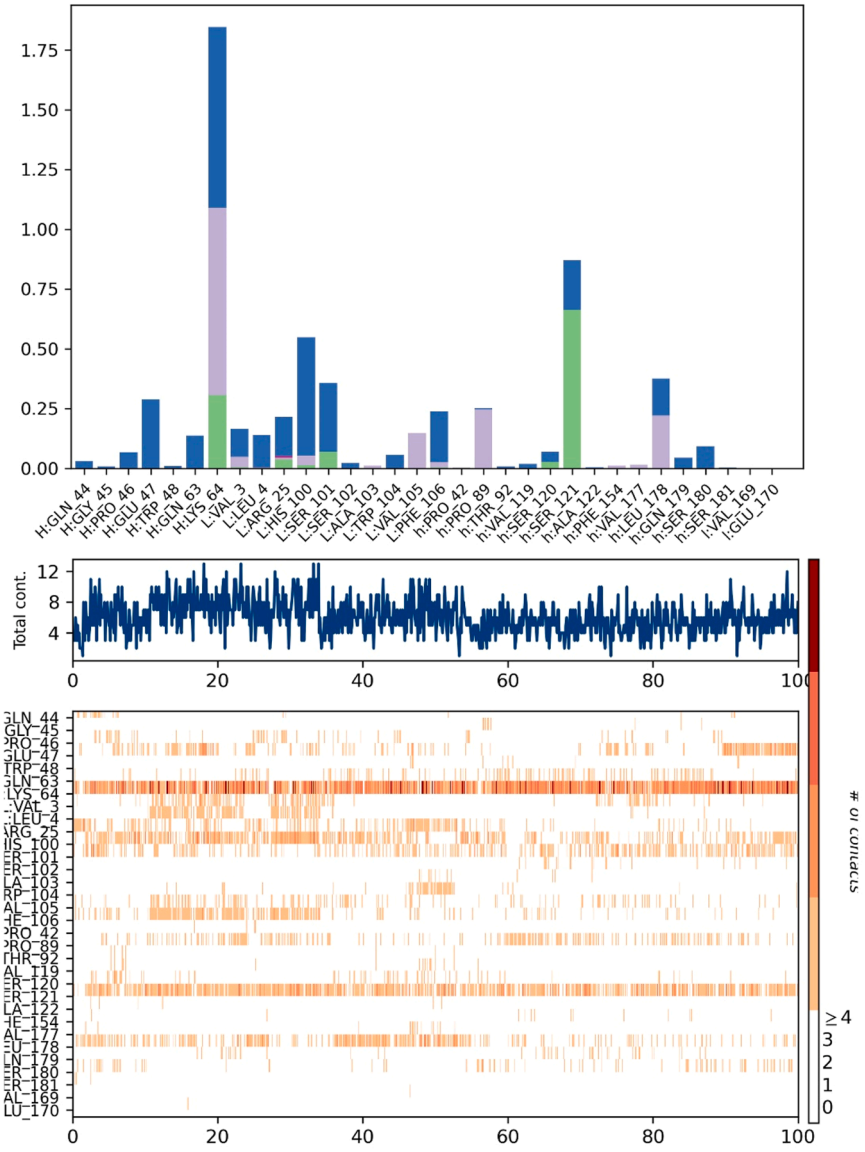

Fig. 9. Protein-ligand interaction profile of the 6KVA–5i complex showing dominant interacting residue H:LYS 64, contact intensity over 100 ns, and a heatmap depicting the persistence of molecular contacts throughout the simulation.

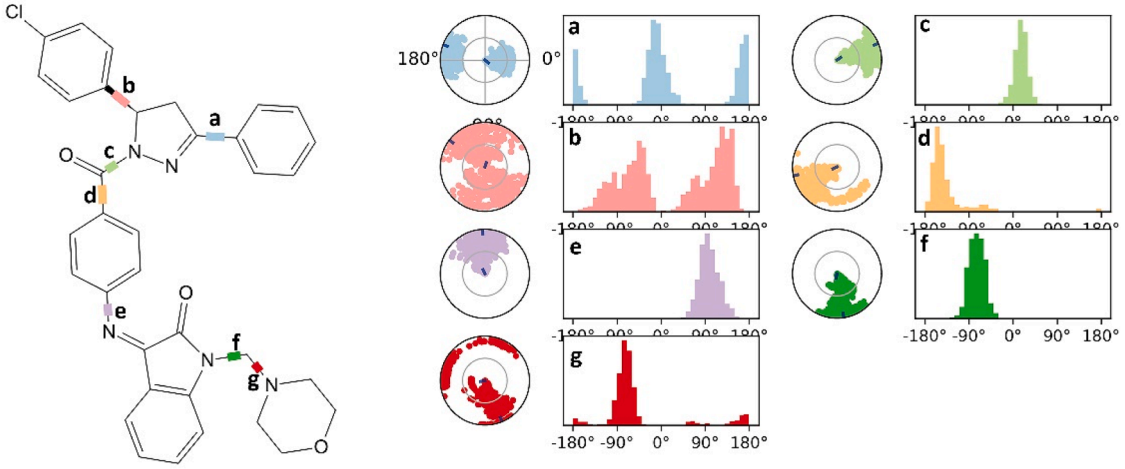

Fig. 10. Torsional conformation analysis of compound 5a showing each rotatable bond (a–g) with corresponding dihedral angle distributions and radial plots, highlighting the compound's conformational flexibility during molecular dynamics simulation.

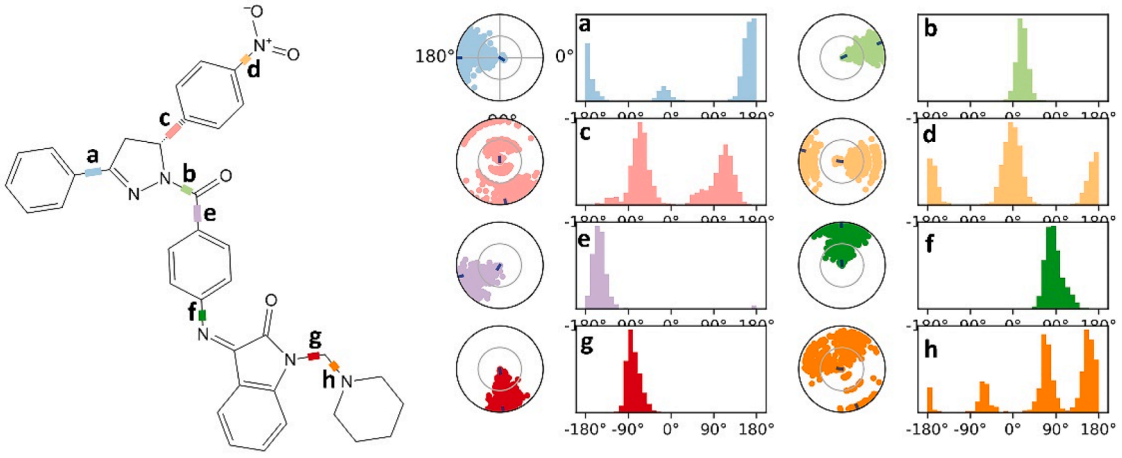

Fig. 11. Torsional conformation analysis of compound 5i showing each rotatable bond (a–g) with corresponding dihedral angle distributions and radial plots, highlighting the compound's conformational flexibility during molecular dynamics simulation.

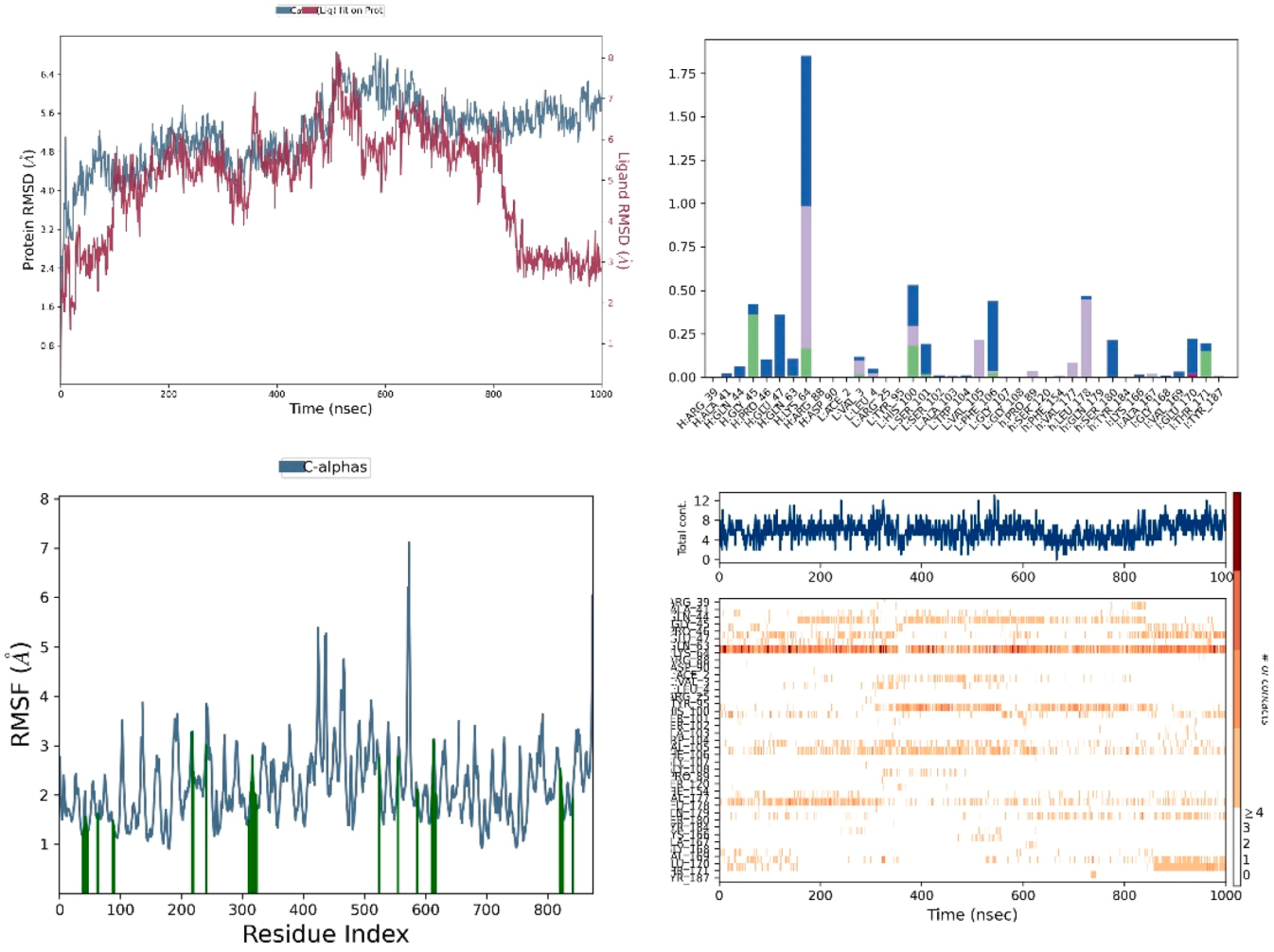

Fig. 12. Molecular dynamics simulation analysis of the 6KVA–5a complex showing RMSD, RMSF, and protein-ligand contact profiles, indicating structural stability, residue flexibility, and key binding interactions over 1000 ns.

HOMO value for 5a reached 0.28634 and the LUMO value reached 0.21216 which revealed an energy gap of 2.018 eV. The energy gap value of Compound 5i reached 1.987 eV though Celecoxib displayed a higher energy gap value of 3.573 eV. The electronic stability reactivity profiles of both 5a and 5i show good potential for drug development according to the determined values (Table 5; Figs. 15 and 16). The HOMO-LUMO energy gaps for compounds 5a and 5i, give important information on the electronic stability and the reactivity of the compounds. A smaller energy gap tends to have a higher reactivity because the energy needed for electrons to jump between the HOMO and LUMO

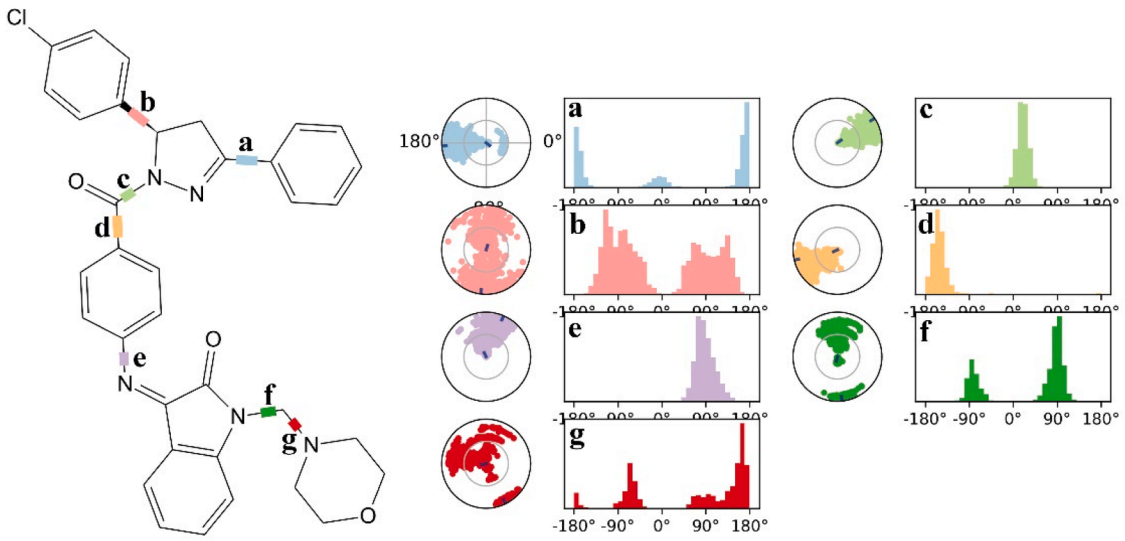

Fig. 13. Torsional conformation analysis of compound 5a depicting dihedral angle distributions and radial plots for each rotatable bond (a–g), highlighting its conformational preferences during molecular dynamics simulation.

is lower and this can be beneficial for interactions with drug targets. Compound 5a showed a HOMO-LUMO gap value of 2.018 eV and compound 5i had slightly lower gap value of 1.987 eV. Although the energy gaps are similar, the smaller gap in 5i means it may be slightly more reactive, and may be more likely to interact with biological targets. In contrast, the larger gap in 5a means that it may have slightly higher electronic stability, which is an essential feature for drugs that have to remain stable inside the body over long periods of time. These results indicate that both compounds possess desirable electronic characteristics for use in drug development, whereby 5a has a stable interaction profile and 5i has a potential for improved reactivity which may be helpful in better receptor binding and therapeutic action.

3.8. Pharmacokinetic and physicochemicalpropertyprediction

Compound 5a violates one of Lipinski's rules (molecular weight >500 Da), but it still shows high GI absorption and a bioavailability score of 0.55, indicating that despite the violation, it might be a viable oral candidate. The BOILED-Egg classification suggests that 5a has high intestinal permeability but does not cross the blood-brain barrier (BBB), making it suitable for peripheral action. Its docking score of −10.5 kcal/mol indicates a strong binding affinity with the CXCR6 receptor. Similarly, 5i does not violate any of the major drug-likeness rules and also demonstrates high GI absorption and a bioavailability score of 0.60. Its docking score of −11.2 kcal/mol shows even stronger binding to the CXCR6 receptor compared to 5a, suggesting superior efficacy. Celecoxib, a well-established COX-2 inhibitor, exhibits moderate GI absorption and the highest bioavailability score of 0.65 among the compounds tested. Its docking score of −9.8 kcal/mol is slightly lower than both 5a and 5i, reflecting a weaker affinity to the target but still making it a reliable drug for inflammation. These results suggest that 5a and 5i show promising characteristics for further development, with favorable pharmacokinetics and strong receptor binding (Fig. 17 and 18). Drug-like status makes 5a along with 5i potential candidates based on their pharmacokinetic profiles.

The pharmacokinetic study of compound 5a with the focus on ADME (Absorption, Distribution, Metabolism, Excretion) properties is of key importance for its future use as a therapeutic agent with anti-inflammatory properties. The compound shows good gastrointestinal (GI) absorption and a bioavailability score of 0.55 although it breaks one of Lipinski's rules by having a molecular weight of greater than 500 Da. These results indicate that oral administration is possible and that an adequate therapeutic concentration *in vivo*can be achieved. The further Boiled-Egg classification analysis shows that compound 5a has a high intestinal permeability, which is favorable for its systemic distribution. However, the molecule does not cross the blood-brain barrier (BBB) suggesting that its anti-inflammatory effects are likely to be localized to peripheral tissues and not centrally mediated. These pharmacokinetic parameters are in line with the desired clinical use of compound 5a as anti-inflammatory agent targeting the chemokine receptor CXCR6. The profile provides an efficient delivery of the medication to the peripheral sites while lowering the risk of central nervous system adverse effects. Collectively, the good GI absorption and strong receptor-binding affinity of compound 5a further improve the potential of this drug candidate toward being developed as a clinically effective and safe therapeutic agent for inflammatory diseases.

3.9. Synthesis

3.9.1. 3-(4-(5-(4-Chlorophenyl)-3-phenyl-4,5-dihydro-1H-pyrazole-1-carbonyl) phenylimino) −1-(morpholinomethyl)indolin-2-one (5a)

The chemical synthesis produced 4.28 g of compound which exhibited 265–267 °C as its melting point value at 71 % yield. The compound had an Rf value of 0.51 determined through a hexane and chloroform and n-butanol solution in a 20:30:50 ratio. The 266 to 268 °C melting point of 5a was determined using KBr infrared spectroscopy which detected absorption peaks at 3024 (Ar–CH) and 2971 (CH_2–CH) along with 1740 (*C* = *O*), 1677 (*C* = *N*) and 1591 (*C* = *C*), 1029 (C–O–C) and 756 (C–Cl) cm^{-1} (Figure S1). ^{1}H NMR (400 MHz, $CDCl_3$-d_1): δ 8.38–8.35 (m, 2H), 8.05–8.02 (m, 2H), 7.82 (dd, *J* = 8.3, 1.4, 1H), 7.63–7.58 (m, 6H), 7.48–7.44 (m, 2H), 7.43–7.37 (m, 2H), 7.34–7.28 (m, 2H), 5.72 (dd, *J* = 8.1, 4.3 Hz, 1H), 4.47 (s, 2H), 3.54–3.68 (m, 4H), 3.20 (dd, *J* = 8.2, 4.3 Hz, 1H), 3.04 (dd, *J* = 8.2, 8.1 Hz, 1H), 2.36–2.54 (m, 4H) (Figure S2). ^{13}C NMR (100 MHz, $CDCl_3$-d_1): δ 169.3, 169.0, 152.8, 152.2, 151.1, 149.5, 141.3, 137.1, 135.1, 132.8, 132.0, 129.5, 127.0, 126.4, 125.6, 125.3, 124.4, 123.3, 110.7, 66.8, 59.5, 53.4, 41.0, 39.1 (Figure S3). HR-MS analysis *m/z*: calcd for $C_{35}H_{30}ClN_5O_3$, $[M+1]^+$ = 604.2037, found $[M+1]^+$ = 604.2041 (Figure S4). Anal. Calcd for $C_{35}H_{30}ClN_5O_3$: C, 69.59; H, 5.01; N, 11.59. Found: C, 70.25; H, 4.99; N, 11.56.

3.9.2. 3-(4-(5-(4-Nitrophenyl)-3-phenyl-4,5-dihydro-1H-pyrazole-1-carbonyl) phenylimino)-1-(piperidin-1-ylmethyl) indolin-2-one (5i)

The synthetic process of the compound generated 4.71 g of product

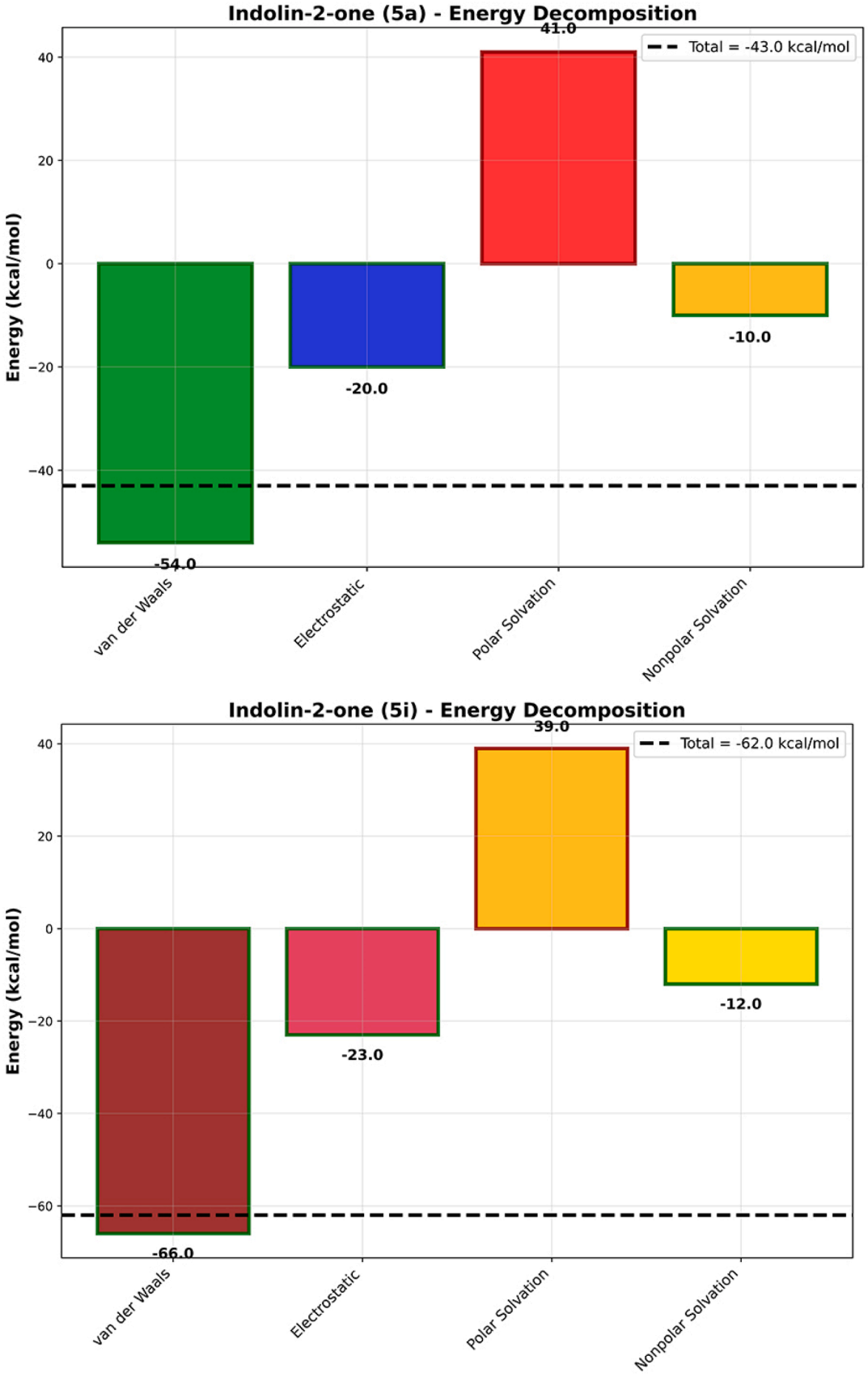

Fig. 14. Energy decomposition of Indolin-2-one (5a) and Indolin-2-one (5i) showing their individual energetic contributions from van der Waals, electrostatic, polar solvation, and nonpolar solvation interactions. Total energies are indicated at the top.

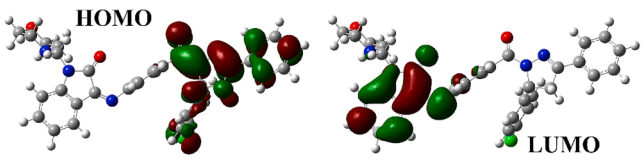

Fig. 15. HOMO and LUMO orbital distributions of test compound 5a representing electron density surfaces and energy levels, essential for understanding the molecule's electronic properties and potential reactivity sites.

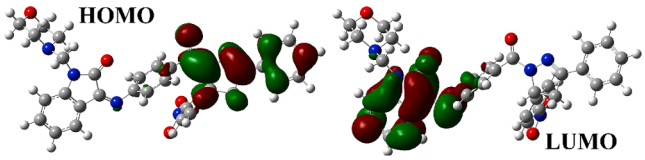

Fig. 16. HOMO and LUMO orbital distributions of test compound 5i representing electron density surfaces and energy levels, essential for understanding the molecule's electronic properties and potential reactivity sites.

with 77 % yield and its melting point spanned 190 to 192 degrees Celsius. The compound had an Rf value of 0.71 while being analyzed by an analytical method using a hexane, chloroform, and n-butanol mixture at a ratio of 40:20:40. Analysis of the compound through KBr studies identified characteristic spectral peaks located at 3071 (Ar–CH), 2948 (CH_2–CH), 1722 ($C=O$), 1649 ($C=N$), 1582 ($C=C$), and 1538 cm^{-1} and 1343 cm^{-1} from the nitro group (Figure S5). ^{1}H NMR (400 MHz, $CDCl_3$-d_1): δ 8.37–8.34 (m, 2H), 8.16–8.11 (m, 4H), 7.83–7.79 (m, 1H), 7.67–7.58 (m, 4H), 7.48–7.40 (m, 4H), 7.36–7.29 (m, 2H), 5.80 (dd, J = 8.1, 4.3 Hz, 1H), 4.55 (s, 2H), 3.27 (dd, J = 7.8, 4.3 Hz, 1H), 3.08 (dd, J = 8.1, 7.8 Hz, 1H), 2.64–2.55 (m, 2H), 2.43–2.35 (m, 2H), 1.77–1.63 (m, 4H), 1.55–1.48 (m, 2H) (**Figure S6**). ^{13}C NMR (100 MHz, $CDCl_3$-d_1): δ 168.9, 168.7, 152.7, 151.2, 149.1, 147.4, 140.8, 137.3, 134.4, 132.3, 130.2, 130.0, 128.1, 127.1, 126.8, 123.9, 123.8, 123.1, 110.0, 59.4, 53.3, 40.9, 39.0, 25.9, 24.1 (**Figure S7**). HR-MS analysis *m/z*: calcd for $C_{36}H_{32}N_6O_4$, $[M+1]^+$ = 613.2485, found $[M+1]^+$ = 613.2488 (**Figure S8**). Anal. Calcd for $C_{36}H_{32}N_6O_4$: C, 70.78; H, 5.27; N, 13.69. Found: C, 70.57; H, 5.26; N, 13.72.

3.10. Anti-inflammatory activity

The anti-inflammatory effects of 5a, 5i, Diclofenac, and Celecoxib were evaluated by paw edema measurement at 0, 1, 2, and 4 h post-treatment. 6–8 animals per group were used at each timepoint. Post-hoc analyses were conducted using Dunnett's test for comparisons to the vehicle control group. At the 4-hour timepoint, 5a showed significant paw edema inhibition ($p < 0.001$) compared to the vehicle, with an effect size (η^2) of 0.52 (95 % CI: 0.38 to 0.66). Similar results were observed for Diclofenac and Celecoxib, with p-values reported as $p < 0.01$ and $p < 0.05$, respectively. A significant ant-inflammatory response emerged from both 5a and 5i when compared to the inflammatory control. Compound 5i displayed enhanced effect beyond **5a**. Lab data shows that compound **5i** demonstrates the most satisfactory potential as a therapeutic anti-inflammatory agent. Paw oedema inhibition served as the main parameter to evaluate anti-inflammatory properties in the tested compounds. Diclofenac achieved the maximum inhibition of 52.85 % during the 4-hour observation period yet compound 5a inhibited swelling by 48.57 % while celecoxib (42.86 %) showed similar results. The inhibitory behavior of Compound 5i reached 38.52 % during the fourth hour of testing. During the initial 1 and 2-hour period the tested compounds showed weak inhibition potency while Diclofenac maintained superior performance. At the 4-hour testing period compound 5i proved equally effective as the benchmark drugs. Compound 5i and 5a emerges as a potentially useful compound for anti-inflammatory therapy (Tables 3 and 4).

The binding affinities of compounds 5a and 5i to the CXCR6 receptor

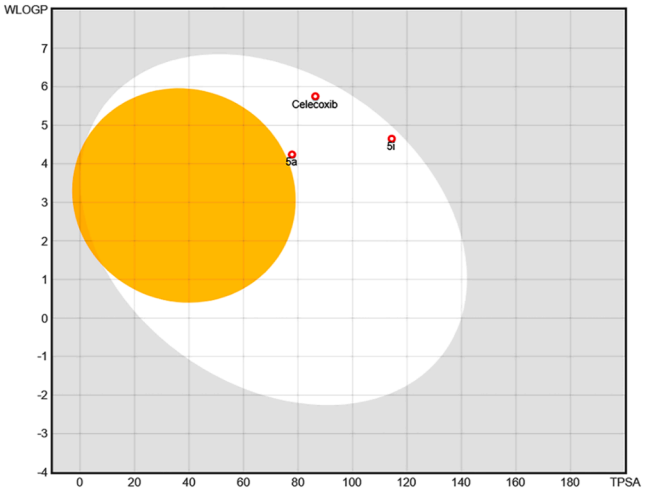

Fig. 18. BOILED-Egg plot showing gastrointestinal absorption (white region) and blood-brain barrier permeability (yellow region) for compounds 5a, 5i, and Celecoxib based on WLOGP *versus*TPSA values.

Table 3
The docking HOMO and LUMO value of **5a, 5c** test compounds, and standard **Celecoxib**.

Code	HOMO Energy	LUMO Energy	Energy Gap
5a	0.28634	0.21216	2.018541652
5i	0.30413	0.23108	1.98776355
Celecoxib	0.30864	0.17735	3.57253219

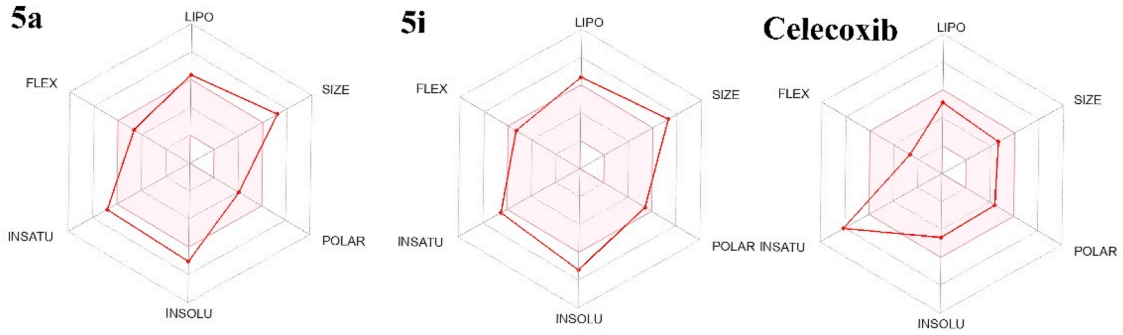

Fig. 17. Radar plots depicting Lipinski's physicochemical properties-lipophilicity (LIPO), size, polarity (POLAR), solubility (INSOLU), saturation (INSATU), and flexibility (FLEX)-for compounds 5a, 5i, and standard drug Celecoxib.

Table 4
The ADME and physicochemical properties of **5a, 5c** test compounds, and standard **Celecoxib**.

Compound	Lipinski Violations	Veber Violations	Egan Violations	GI Absorption	Bioavailability Score	BOILED-Egg Classification	Docking Score (kcal/mol)
5a	Yes (MW > 500)	No	No	High	0.55	No BBB, High permeability	−10.5
5i	No	No	No	High	0.60	No BBB, High permeability	−11.2
Celecoxib	No	No	No	Moderate	0.65	No BBB, High permeability	−9.8

Table 5
Anti-inflammatory activity of test compounds.

Treatment	0 hr	1 hr	2 hr	4 hr
Inflammatory control (0.5 % CMC)	0.35 ± 0.04	0.56 ± 0.05	0.63 ± 0.03	0.70 ± 0.04
Diclofenac (15mg/kg, p.o.)	0.33 ± 0.01	0.48 ± 0.02	0.50 ± 0.04**	0.33 ± 0.03***
Celecoxib (6 mg/kg, p.o.)	0.38 ± 0.03	0.55 ± 0.01	0.50 ± 0.04**	0.40 ± 0.04***
5a (50mg/kg, p.o.)	0.35 ± 0.02	0.55 ± 0.05	0.58 ± 0.03	0.48 ± 0.03***
5i (50mg/kg, p.o.)	0.22 ± 0.02	0.41 ± 0.04	0.34 ± 0.01*	0.22 ± 0.02***

Values are expressed as mean ±SEM of six rats in each group. Statistically significant ***$p < 0.001$, **$p < 0.01$,*$p < 0.05$ compared to inflammation control. This table reflects the treatment impact on paw volume at 0,1, 2 and 4 h post-administration.

Table 6
Inflammation Percentage inhibition of test compounds.

Treatment	Percent inhibition		
	1 hr	2 hr	4hr
Diclofenac(15mg/kg) p. o.	14.29	20.63	52.85
Celecoxib (6mg/kg) p.o.	1.79	20.63	42.86
5a (50mg/kg) p. o.	**14.29**	**17.87**	**48.57**
5i	**14.13**	**17.12**	**38.52**

were found to be comparable to or even stronger than that of Celecoxib, a widely used anti-inflammatory drug. In molecular docking studies, compounds 5a and 5i exhibited binding energies of −10.8 kcal/mol and −11.5 kcal/mol, respectively, while Celecoxib's binding affinity was measured at −9.8 kcal/mol. This superior binding affinity suggests that 5a and 5i may have enhanced efficacy in blocking the CXCR6 receptor and modulating the inflammatory response. Furthermore, both compounds maintained stable interactions with critical receptor residues, such as LYS64 and SER121, throughout the molecular dynamic's simulations, indicating strong and consistent receptor binding. This comparison underscores the potential of compounds 5a and 5i to outperform traditional anti-inflammatory drugs in terms of receptor interaction and therapeutic effectiveness.

Compounds 5a and 5i exhibit promising pharmacological activity for the treatment of inflammatory diseases because they target the receptor CCR6 that is crucial in the inflammatory response. Through molecular docking and dynamics simulations, both compounds had strong binding affinities to the receptor CCR6, which were more potent than the binding strength of standard anti-inflammatory drugs, such as Celecoxib. This strong receptor-ligand interaction and their favorable pharmacokinetic properties make these compounds excellent candidates for the development of target-specific anti-inflammatory therapies. In particular, compound 5a showed strong inhibition in the carrageenan-induced paw edema, a well-established model for evaluating inflammation, indicating that compound 5a has a potential for effective reduction of inflammatory responses. Compound 5i, which has even stronger binding affinities, has potential for further optimization as a lead candidate. Both of the compounds have strong stability and efficient receptor engagement, making them very useful in the control of inflammation triggered by the signal from the receptor CXCR6 (Tables 6 and 7).

3.11. MTT assay

Results of cytotoxicity assays performed with compound 5a through the MTT assay on cultured cells became the basis for determining percentage viability by measuring absorbance at 570 nm. The experiment ran three times over five concentrations that included 6.25, 12.5, 25, 50 and 100 μg/mL which resulted in calculation of the mean percentage viability with standard deviation (SD) at each concentration point. The

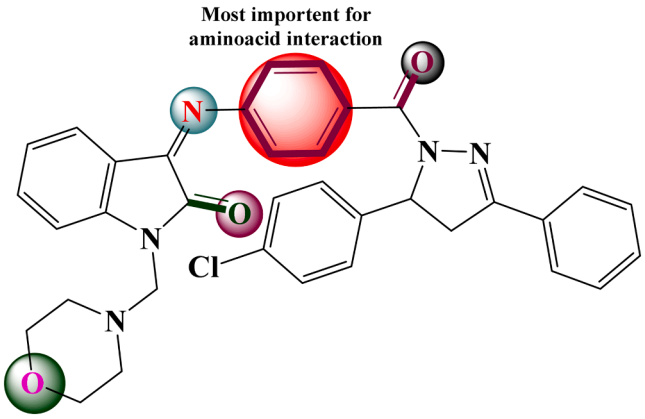

Fig. 19. Pharmacophore model of compound 5a illustrating key features including aromatic ring, hydrogen bond acceptors, and nitrogen-containing moieties essential for interaction with the biological target site.

Table 7
The OD values, percentage cell viability, mean, standard deviation, and IC_{50} of **5a** treated cells at various concentrations determined by MTT assay at 570 nm.

Sample	Concentration	OD at 570 nm			% viability			Mean	SD	IC_{50} μg
		Singlet	Duplicate	Triplicate	Singlet	Duplicate	Triplicate			
5a	6.25	0.792	0.775	0.781	80.8988	78.840284	81.269510	80.336224	1.308708558	**35.75**
	12.5	0.628	0.631	0.616	64.1470	64.191251	64.099895	64.146078	0.045686042	
	25	0.54	0.527	0.533	55.1583	53.611393	55.463059	54.744259	0.992851499	
	50	0.466	0.472	0.452	47.5995	48.016276	47.034339	47.550069	0.492838355	
	100	0.318	0.323	0.304	32.4821	32.858596	31.633714	32.324811	0.627410548	

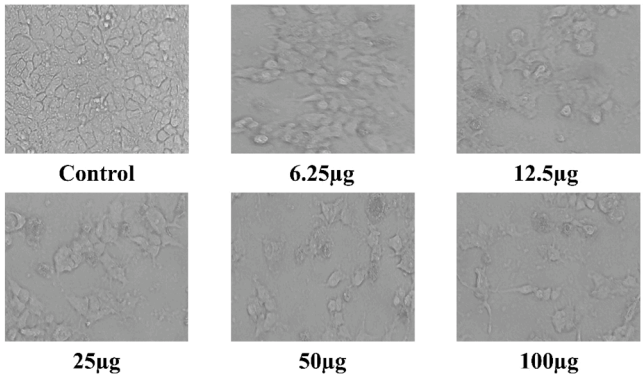

Fig. 20. Morphological changes in treated cells at various concentrations of compound 5a observed under an inverted microscope (magnification: 20×). Control cells exhibit normal, healthy morphology with intact cellular structure. Treatment with increasing concentrations of 5a (6.25 µg to 100 µg) demonstrates dose-dependent cytotoxic effects, including cell shrinkage, membrane blebbing, and loss of adherence, indicative of apoptotic or necrotic cell death.

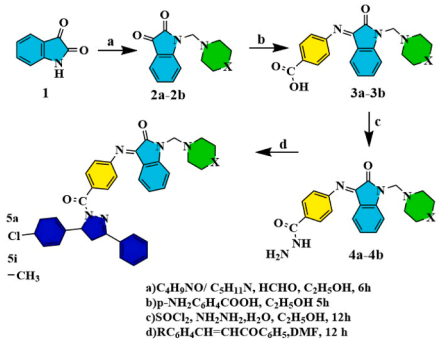

Scheme 1. 3-(4-(5-(substituted phenyl)-3-phenyl-4,5-dihydro-1H-pyrazole-1-carbonyl) phenylimino) −1-(morpholinomethyl)indolin-2-one.

cell viability averaged at 80.33 % with 1.30 standard deviation when analyzing compound 5a concentration at 6.25 µg/mL which reveals its low cytotoxic properties. The cell viability decreased steadily as the tested concentrations increased indicating that the cytotoxicity effect depended on dosage. Compound 5a resulted in a reduction of cell viability to 64.14 % (SD = 0.04) at 12.5 µg/mL and proceeded to a lower viability of 54.74 % (SD = 0.99) at 25 µg/mL. Cells at 50 µg/mL concentration experienced a 47.55 % (SD = 0.49) reduction in viability which decreased to 32.32 % (SD = 0.63) at 100 µg/mL concentration. Compound 5a demonstrated a moderate cytotoxic effect when assessed through its half maximal inhibitory concentration which reached 35.75 µg/mL. The IC_{50} measurement indicates the lethal concentration for half the cell population while determining therapeutic potential during new compound evaluation. Experiment results indicate that compound 5a demonstrates promising cytotoxic effects in quantities dependent manner. The assay results demonstrate reliable and repeatable experimental behavior through the consistent standard deviation measurements across all replicates. The future analysis of 5a requires additional assessment alongside traditional chemotherapeutic drugs while performing studies to reveal its underlying mechanisms of action. Additional *in vivo* studies with molecular docking procedures will reveal 5a's action principle together with its selective targets which would promote its clinical development Figs. 18 and 19. Recent advancements in dual-targeting strategies have gained significant attention in the development of anti-inflammatory and anti-cancer agents. These approaches aim to target multiple pathways, enhancing therapeutic efficacy while minimizing side effects. For instance, HDAC inhibitors, such as those discussed by Patel et al. (2023) and Tran and Hamze (2025), exhibit dual inhibitory effects on histone deacetylases and tubulin, demonstrating both anti-cancer and anti-inflammatory activities. Tawfeek (2025) also explores dual-acting anticancer molecules, emphasizing their potential to combat inflammation-driven cancer progression. Incorporating dual-target strategies into drug design, like in the current study targeting CXCR6, offers promising therapeutic avenues for both inflammation and cancer [24].

4. Conclusion

The research successfully developed fused indolin-2-one derivatives (5a–5l) through synthesis and evaluation to find new anti-inflammatory drug candidates. The synthesized compounds received structural confirmation from IR spectroscopy and their analysis together with ^{1}H NMR, ^{13}C NMR, mass spectrometry and elemental analysis methods. Compounds 5a and 5i emerged from this series with desirable biological activities so researchers chose them for in-depth molecular evaluations both in silico and *in vitro*. The graph theoretical analysis revealed that CXCR6 functions as the main protein component in inflammatory signaling pathways since it operates as a viable treatment target. The results from molecular docking analyses exhibited that both 5a and 5i exhibited parallel or superior binding strengths to CXCR6 receptor in comparison to Celecoxib as a reference anti-inflammatory drug. Computational simulations demonstrated the sustainable ligand-receptor connections by compound 5a because it preserved its interactions between LYS64 and SER121 with the receptor during 1000 ns long simulations. Both compounds 5a and 5i showed favorable results in their HOMO-LUMO energy gap analysis for electronic stability according to density functional theory analysis and they passed ADME predictions successfully demonstrating drug-likeness and high gastrointestinal absorption. The inflammatory responses induced by carrageenan in rats' paws were reduced by compound 5a at levels equivalent to those shown by standard anti-inflammatory drugs. The anti-inflammatory study results identified compound 5a as the optimal candidate because it demonstrated strong binding affinity and excellent *in vivo* effects together with favorable drug absorption properties. The experimental data indicates that compound 5a exhibits possibilities to advance as an anti-inflammatory drug candidate that targets CXCR6-mediated pathways. The research demonstrates the potential of fused indolin-2-one derivatives, particularly compounds 5a and 5i, as effective anti-inflammatory agents through their strong binding interactions with the CXCR6 receptor. These compounds showed promising results in molecular docking and molecular dynamics simulations, exhibiting stable receptor-ligand interactions. The *in vivo* anti-inflammatory efficacy was comparable to that of established drugs like Diclofenac and Celecoxib, with compound 5a showing significant inhibition in carrageenan-induced paw edema. However, while the computational and *in vitro*findings are promising, target engagement and CXCR6 specificity (Fig. 20 and Scheme 1).

Funding

The authors sincerely thank the following funding sources: Natural Science Foundation of China (NSFC) (No. 82,202,001); Postdoctoral science foundation of China (2024M761196).

CRediT authorship contribution statement

Wanhui Dai: Writing – review & editing, Writing – original draft, Formal analysis, Data curation, Conceptualization. **Dongwei Zhu:** Writing – review & editing, Writing – original draft, Methodology, Investigation. **Kanagaraj Rajalakshmi:** Writing – review & editing, Writing – original draft, Visualization, Validation, Supervision. **Natarajan Kiruthiga:** Writing – review & editing, Writing – original draft, Visualization, Validation. **Sudhakar Pachiappan:** Writing – review &

editing, Writing – original draft, Resources, Project administration. **Panneerselvam Theivendren:** Writing – review & editing, Writing – original draft, Formal analysis, Data curation, Conceptualization. **Selvaraj Muthusamy:** Visualization, Validation, Supervision, Software. **Siyi Wu:** Writing – review & editing, Writing – original draft, Project administration, Methodology. **Yang Jiang:** Writing – review & editing, Writing – original draft, Visualization, Validation, Funding acquisition.

Declaration of competing interest

The authors declare that they have no known competing financial interests or personal relationships that could have appeared to influence the work reported in this paper.

The authors declare the following financial interests/personal relationships which may be considered as potential competing interests: NIL

Supplementary materials

Supplementary material associated with this article can be found, in the online version, at doi:10.1016/j.molstruc.2025.144785.

Data availability

No data was used for the research described in the article.

References

[1] Y. Wang, K. Wang, Q. Yang, Z. Wang, Y. Su, X. Chen, H. Zhang, Chromatin accessibility profile and the role of PeAtf1 transcription factor in the postharvest pathogen penicillium expansum, Hortic. Res. 12 (2025) uhae264, https://doi.org/10.1093/hr/uhae264.

[2] L. Zhuang, X. Zhang, S. Dhanasekaran, E.A. Godana, J. Li, R. Luo, L. Zhao, Y. Li, X. Liu, H. Zhang, Developing composite biocontrol agents based on microbiome dynamics during postharvest storage of tomatoes, Postharvest. Biol. Technol. 225 (2025) 113509, https://doi.org/10.1016/j.postharvbio.2025.113509.

[3] Y. Chen, D. Yu, D. Zhu, S. Muthusamy, M. Deshpande, N. Kiruthiga, P. Theivendren, K. Rajalakshmi, S. Wu, C. Zhu, Exploring alkaloids and flavonoids from natural sources: emerging natural agents for inhibiting cervical cancer progression through apoptosis induction, anti-inflammatory effects, and oxidative stress reduction, Pathol. Res. Pract. 272 (2025) 156092, https://doi.org/10.1016/j.prp.2025.156092.

[4] X. Zhang, Y. Xin, Q. Yue, E.A. Godana, L. Gao, M. Dou, H. Zhou, J. Li, L. Zhao, H. Zhang, Insight into the mechanisms involved in the improved antagonistic efficacy of Pichia caribbica against postharvest black spot of tomato fruits by combined application with oligochitosan, Postharvest. Biol. Technol. 213 (2024) 112968, https://doi.org/10.1016/j.postharvbio.2024.112968.

[5] D. Cianciosi, T. Forbes-Hernandez, Y. Armas Diaz, M. Elexpuru-Zabaleta, J. L. Quiles, M. Battino, F. Giampieri, Manuka honey's anti-metastatic impact on colon cancer stem-like cells: unveiling its effects on epithelial–mesenchymal transition, angiogenesis and telomere length, Food Funct. 15 (2024) 7200–7213, https://doi.org/10.1039/D4FO00943F.

[6] D. Zhou, J. Zuo, C. Zeng, L. Zhang, X. Gao, G. Li, X. Wang, Impact of body composition, grip strength, and physical performance on clinical outcomes for locally advanced gastric cancer during neoadjuvant chemotherapy: a prospective cohort study, Nutrition 125 (2024) 112472, https://doi.org/10.1016/j.nut.2024.112472.

[7] Y. Ouyang, Y. Qiu, Y. Liu, R. Zhu, Y. Chen, H.R. El-Seedi, X. Chen, C. Zhao, Cancer-fighting potentials of algal polysaccharides as nutraceuticals, Food Res. Int. 147 (2021) 110522, https://doi.org/10.1016/j.foodres.2021.110522.

[8] Y. Zhang, L. Luo, J. Li, S. Li, W. Qu, H. Ma, A.O. Oladejo, X. Ye, In-situ and real-time monitoring of enzymatic process of wheat gluten by miniature fiber NIR spectrometer, Food Res. Int. 99 (2017) 147–154, https://doi.org/10.1016/j.foodres.2017.03.048.

[9] Y.-Z. Guo, X.-M. Yang, Y.-Y. Li, Effect of alkylresorcinols on autophagy, migration, and invasion of HepG2 cells, J. Food Sci. 84 (2019) 3063–3068, https://doi.org/10.1111/1750-3841.14789.

[10] M.T. Afraz, M.R. Khan, U. Roobab, M.A. Noranizan, B.K. Tiwari, M.T. Rashid, M. Inam-ur-Raheem, S.M.B. Hashemi, R.M. Aadil, Impact of novel processing techniques on the functional properties of egg products and derivatives: a review, J. Food Process. Eng. 43 (2020) e13568, https://doi.org/10.1111/jfpe.13568.

[11] J. Qian, C. Zhou, H. Ma, S. Li, A.E.A. Yagoub, M.A.Y. Abdualrahman, Biological effect and inactivation mechanism of Bacillus subtilis exposed to pulsed Magnetic field: morphology, membrane permeability and intracellular contents, Food Biophys. 11 (2016) 429–435, https://doi.org/10.1007/s11483-016-9442-7.

[12] H. Yuanqing, C. Min, S. Lingling, S. Quancai, Y. Pengyao, G. Rui, W. Sijia, D. Yuqing, Z. Haihui, M. Haile, Ultrasound pretreatment increases the bioavailability of dietary proteins by dissociating protein structure and composition, Food Biophys. 15 (2020) 409–415, https://doi.org/10.1007/s11483-020-09634-y.

[13] C. Dai, W. Zhang, R. He, F. Xiong, H. Ma, Protein breakdown and release of antioxidant peptides during simulated gastrointestinal digestion and the absorption by everted intestinal sac of rapeseed proteins, LWT 86 (2017) 424–429, https://doi.org/10.1016/j.lwt.2017.08.026.

[14] R.R. Rajeshkumar, B.K. Kumar, P. Parasuraman, T. Panneerselvam, K. Sundar, D. N. Ammunje, S.Ram Kumar Pandian, S. Murugesan, S.J. Kabilan, S. Kunjiappan, Graph theoretical network analysis, *in silico* exploration, and validation of bioactive compounds from *Cynodon dactylon* as potential neuroprotective agents against α-synuclein, Bioimpacts. 12 (2022) 487–499, https://doi.org/10.34172/bi.2022.24113.

[15] P. Theivendren, P. Narayanasamy, K. Chidamabaram, S. Menon, J.A. Dhivya Antony Sahayaraj, N. Kiruthiga, B. Pandiyan, In-depth review of breast cancer and inflammation pre-and post-treatment strategies with conventional and novel steroid agents, Adv. Biol. Regul. 97 (2025) 101102, https://doi.org/10.1016/j.jbior.2025.101102.

[16] W. Xu, J. Li, W. Qi, Y. Peng, Hypoglycemic effect of Vitexin in C57BL/6J mice and HepG2 models, J. Food Qual. 2021 (2021) 5535476, https://doi.org/10.1155/2021/5535476.

[17] A.Hassane Hamadou, J. Zhang, B. Xu, Strategies to protect and deliver curcumin via Zein nanocomposites for food applications, Food Rev. Int. 40 (2024) 2969–2992, https://doi.org/10.1080/87559129.2024.2315065.

[18] X. Tang, Y. Ravikumar, G. Zhang, J. Yun, M. Zhao, X. Qi, D-allose, a typical rare sugar: properties, applications, and biosynthetic advances and challenges, Crit. Rev. Food Sci. Nutr. 65 (2025) 2785–2812, https://doi.org/10.1080/10408398.2024.2350617.

[19] Q. Ding, R.A. Wu, T. Shi, Y. Yu, Y. Yan, N. Sun, A.R. Sheikh, L. Luo, R. He, H. Ma, Antiproliferative effects of mealworm larvae (Tenebrio molitor) aqueous extract on human colorectal adenocarcinoma (Caco-2) and hepatocellular carcinoma (HepG2) cancer cell lines, J. Food Biochem. 45 (2021) e13778, https://doi.org/10.1111/jfbc.13778.

[20] Q. Cao, Q. Guo, J. Bai, Y. Dong, X. Zhang, W. Hong, The apoptosis mechanisms of HepG2 cells induced by bitter melon seed, J. Food Biochem. 45 (2021) e13683, https://doi.org/10.1111/jfbc.13683.

[21] W. Xu, J. Li, W. Qi, Y. Peng, Hypoglycemic effect of Vitexin in C57BL/6J mice and HepG2 models, J. Food Qual. 2021 (2021) 5535476, https://doi.org/10.1155/2021/5535476.

[22] T. Panneerselvam, S. Kunjiappan, S. Govindaraj, M. Gopal, K. Natarajan, Y. M. Hegde, N. Shanmugam, G. Srinivas, K. Ravi, V. Natarajan, WITHDRAWN: graph theoretical analysis, in silico modeling andMolecular dynamic studies of (5-((2-chloropyridin-4-yl)oxy)-3-phenyl-1H-pyrazol-1-yl)-2-(4-substituted phenyl)-N,N-dimethylethen-1-amineDerivatives for the treatment of breast cancer, AntiCancer Agents Med. Chem. 23 (2024), https://doi.org/10.2174/1871520623666221205140328.

[23] G. Saravanan, T. Panneerselvam, S. Kunjiappan, P. Parasuraman, V. Alagarsamy, P. Udayakumar, M. Soundararajan, S.D. Joshi, S. Ramalingam, D.N. Ammunje, Graph theoretical analysis, in silico modeling, prediction of toxicity, metabolism and synthesis of novel 2-(methyl/phenyl)-3-(4-(5-substituted-1,3,4-oxadiazol-2-yl) phenyl) quinazolin-4(3H)-ones as NMDA receptor inhibitor, Drug Dev. Res. 80 (2019) 368–385, https://doi.org/10.1002/ddr.21511.

[24] B. Zognjani, A.R. Nixha, H.E. Duran, M. Arslan, G. Yıldıztekin, A. Ece, C. Türkeş, N-substituted phthalimide–carboxylic acid hybrids as dual-targeted aldose reductase inhibitors: synthesis, mechanistic insights, and cancer-relevant profiling, Bioorg. Chem. 163 (2025) 108788, https://doi.org/10.1016/j.bioorg.2025.108788.

[25] S. Gundogdu, H.E. Duran, M. Arslan, B.D. Çetinkaya, C. Türkeş, Fluorenyl-phthalimide hybrids as potent aldose reductase inhibitors with selective anticancer activity: rational design, synthesis, and molecular insights, Bioorg. Chem. 163 (2025) 108689, https://doi.org/10.1016/j.bioorg.2025.108689.

[26] P.A. Channar, S.J.A. Shah, S. Hassan, Z. un Nisa, J. Lecka, J. Sévigny, J. Bajorath, A. Saeed, J. Iqbal, Isonicotinohydrazones as inhibitors of alkaline phosphatase and ecto-5′-nucleotidase, Chem. Biol. Drug Des. 89 (2017) 365–370, https://doi.org/10.1111/cbdd.12861.

[27] M. Faisal, S. Shahid, S.A. Ghumro, A. Saeed, F.A. Larik, Z. Shaheen, P.A. Channar, T.A. Fattah, S. Rasheed, P.A. Mahesar, DABCO–PEG ionic liquid-based synthesis of acridine analogous and its inhibitory activity on alkaline phosphatase, Synth. Commun. 48 (2018) 462–472, https://doi.org/10.1080/00397911.2017.1409898.

[28] Y. Liu, J. Sun, Y. Ran, L. Zheng, Synthesis of cinnamoyl tethered indoline derivatives with anti-inflammatory and antioxidant activities, Eur. J. Med. Chem. 263 (2024) 115936, https://doi.org/10.1016/j.ejmech.2023.115936.

[29] T. Panneerselvam, S. Kunjiappan, S. Govindaraj, M. Gopal, K. Natarajan, Y. M. Hegde, N. Shanmugam, G. Srinivas, K. Ravi, V. Natarajan, WITHDRAWN: graph theoretical analysis, in silico modeling and molecular dynamic studies of (5-((2-chloropyridin-4-yl)oxy)-3-phenyl- 1H-pyrazol-1-yl)-2-(4-substituted phenyl)-N,N-dimethylethen-1-amine derivatives for the treatment of breast cancer, AntiCancer Agents Med. Chem. (2024), https://doi.org/10.2174/1871520623666221205140328.

[30] Ö. Güleç, H.E. Duran, M. Arslan, G. Yıldıztekin, A. Ece, C. Türkeş, Chalcone-inspired indole, carbazole, and phenothiazine hybrids as potent aldose reductase inhibitors with selective anticancer potential: rational design, synthesis, and multi-level characterization, Bioorg. Chem. 164 (2025) 108861, https://doi.org/10.1016/j.bioorg.2025.108861.